Effects of External Compression on an Axisymmetric Turbulent Near Wake

D.H. Neale,* J.E. Hubbartt,† W.C. Strahle,‡ and W.W. Wilson§
Georgia Institute of Technology, Atlanta, Ga.

An experimental study of base flows for a 5.715-cm-diam projectile at Mach 3 with and without disturbances simulating external burning is reported. Base pressure and wake structure measurements from systematic variations in axisymmetric external compression fields show that substantial base thrust can be produced and that the pressure and length scales of the external disturbances are imposed on the near wake. Measurements with comparable axisymmetric and asymmetric compression contours show that peripherial gradients reduce the base pressure rise. Furthermore, relatively large changes in the near wake length scales and a slight reduction in the base pressure occur when the solid-body blockage effects of discrete radial fuel jets are modeled with pegs mounted near the base of the test projectile.

Nomenclature

$\mathfrak{L}$ = centerline
M = Mach number
P = pressure
R = model radius
X = axial coordinate
U = axial velocity
η = transformed incompressible radial coordinate
θ = boundary-layer momentum thickness

Subscripts

1 = undistributed freestream value
01 = undistributed freestream stagnation value
b = base
e = value at outer edge of shear layer
p = pitot value

Superscript

$\bar{(\ )}$ = mean value

I. Introduction

THERE are a great number of potential air-to-air, air-to-ground, and ground-to-air weaponry missions that require either a sustain or mild acceleration segment of the missile trajectory or which could benefit from substantial drag reduction during a portion of the flight path. Many of these missions require operation sufficiently low in the atmosphere that airbreathing propulsion is attractive, provided that it is competitive with the rocket. Recent concepts appear to make external burning for propulsion a prime candidate for these applications. The elimination of an inlet, combustion chamber, and nozzle for such systems offers significant vehicle simplification with an acceptable sacrifice in I_{sp} when compared with the usual airbreathing apparatus.

Strahle[1] introduced one currently promising major concept of external burning for bluff-base bodies. This concept calls for radial injection and ignition of fuel in the exterior inviscid flow just upstream of the projectile base plane. Strahle's analysis predicted that the resulting combustion-generated elevated pressures in the exterior flow downstream of the base would feed back to the projectile through the subsonic wake region yielding a reduction in base drag.

Theoretical and experimental support for this concept has been provided by Smithey.[2] External burning was simulated in tests at Mach 2 by imposing a compression field on the wake region with exterior nozzle contours. Smithey's measurements of base pressure revealed that 1) net thrust can be generated by external burning, 2) the heat release region should be located such that compression waves impinge on the projectile slightly ahead of the base and 3) for a fixed total heat release, the heating zone length should be minimized.

The analyses of both Strahle and Smithey employed a form of the Crocco-Lees[3] theory for base flows and confined combustion to the inviscid portion of the flow. In practice, however, combustion will become entrained in the shear layer and will give a significantly more complex base flowfield. Until recently, no analysis existed that seriously attempted to treat these complicated flows. Current high interest in the field is reflected in the literature, however, with the appearance of several analytical[4,5] and experimental[6-8] investigations of base flows with external combustion.

A major impediment in the understanding and solution of base flows with radial fuel injection and external combustion is the lack of comprehensive experimental data reflecting systematic alterations in the external flowfield against which theory may be tested. This is particularly true in the area of base flow structure as revealed by detailed measurements in the near wake. The present paper describes the results of the first phase of an experimental test program designed to provide base pressures and near wake structure for systematic variations in simulated external burning.

II. Test Facility

The present blowdown-type test facility was designed to simulate the base flow of a projectile at Mach 3 with a fineness ratio of about 6 and a Reynolds number, based on model diameter, of 3.0×10^6. In addition, the facility design includes provisions for generating and exposing the base flow to disturbances simulating those expected with external burning for propulsion.

Presented as Paper 77-925 at the AIAA/SAE 13th Propulsion Conference, Orlando, Fla., July 11-13, 1977; submitted July 29, 1977; revision received April 28, 1978.

Index categories: Jets, Wakes, and Viscid-Inviscid Flow Interactions; Airbreathing Propulsion.

*Senior Research Engineer, School of Aerospace Engineering.
†Professor of Aerospace Engineering, School of Aerospace Engineering. Member AIAA.
§Regents' Professor, School of Aerospace Engineering, Member AIAA.
§Student Research Assistant, School of Aerospace Engineering. Now employed with General Dynamics Corp., Fort Worth, Texas. Member AIAA.

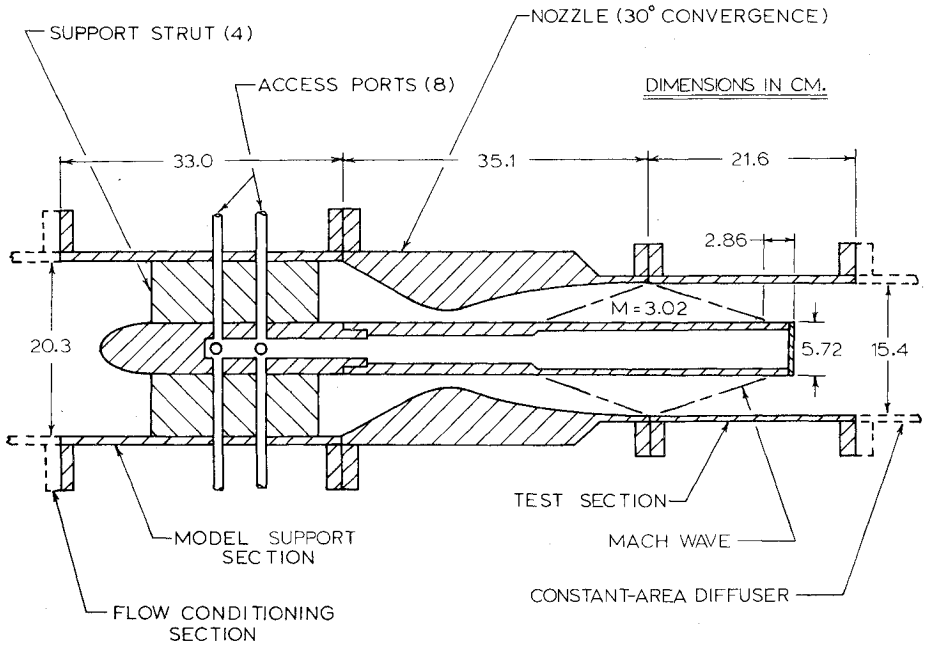

Fig. 1 Base flow facility test section detail.

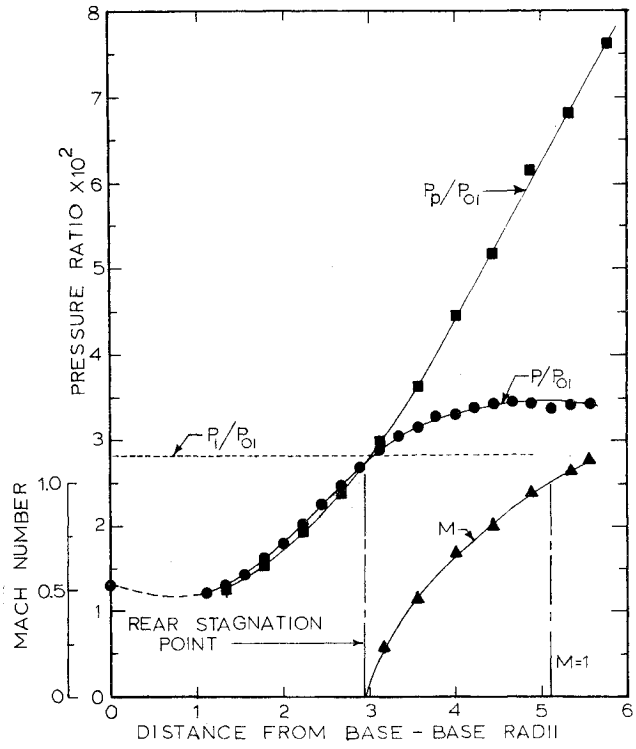

Fig. 2 Near-wake centerline pressure and Mach number distribution—constant-area test section (zero external compression).

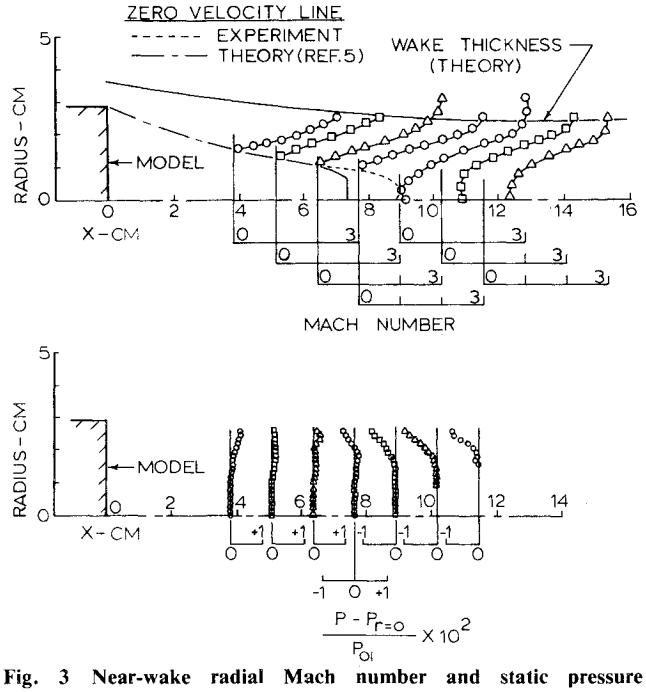

Fig. 3 Near-wake radial Mach number and static pressure distributions—constant-area test section (zero external compression).

Test section details are shown in Fig. 1. The cylindrical model is supported in the upstream subsonic flow and extends through the throat into a transparent test section. Model instrumentation includes seven static pressure taps located on the base, sixteen static pressure taps on the side walls and two thermocouples bonded to the inner wall surfaces near the base plane. Thirty-three additional surface static taps are distributed along the tunnel walls from the nozzle exit plane to the constant area diffuser discharge. Detailed flowfield surveys in the model wake are made using standard telescoping pitot and static probes introduced downstream of the test section through the diffuser wall. Probe positioning and data sampling are computer controlled.

III. Experimental Results

Flow and Measurement Accuracy Evaluation

A comprehensive program of calibration and testing was conducted with the present facility to establish data and flow quality before detailed base flow measurements were attempted. The test section operated repeatedly within 1% of design Mach number as determined by static pressure measurements taken on the model and outer duct surfaces. It was further determined that pressure measurements were accurate within ±1% including wake and freestream static pressures that were typically less than 3 psia. In addition, it was demonstrated that the base flows were free of diffuser and probe interference effects and unaffected by a doubling of the Reynolds number. Data quality review continued throughout the testing program with frequent checks for transducer calibration and for flow symmetry and

repeatability. Special attention was given to identifying and tracing disturbances generated by deliberate variations in the model base and test section wall configurations. Such care was deemed critical in assuring that measured base pressures and wake flow details were representative of free flight conditions and were not contaminated by disturbances reflected from the tunnel walls into the subsonic wake region.

Zero External Disturbance Studies

An initial series of detailed wake measurements was performed using a constant-diameter test section to simulate base flow with no external disturbances other than those due to centerbody and outer duct boundary layers. The theoretical boundary-layer momentum thickness on the model at the base plane was 1.2% of the model radius for a nominal test Reynolds number, based on centerbody diameter, of 2.7×10^6. Computation of the outer duct boundary layer at the nozzle exit showed similarly small characteristic dimensions.

Figures 2 and 3 present typical test measurements conducted in the wake region. Figure 2 shows pitot and static pressure distributions along the model centerline downstream of the base. The corresponding centerline Mach number aft of the rear stagnation point is also displayed. P_l and P_{0l} denote the static and stagnation pressures in the freestream immediately ahead of the base plane. P and P_p are the probe-measured static and pitot pressures, and M is the calculated Mach number. All pressures have been normalized by P_{0l} measured almost simultaneously to minimize the effects of stagnation pressure drifts.

The rear stagnation point, determined from the intersection of the pitot and static pressure curves, is also specified in Fig. 2. In addition, Fig. 2 shows the smooth centerline flow acceleration from stagnation through sonic velocity. Finally, the ratio of static to stagnation pressure upstream of the base, P_l/P_{0l}, is included for comparison with the centerline static pressure distribution to illustrate the overcompression that occurs near the wake neck for axisymmetric base flow. This overcompression is primarily responsible for the higher base pressure demonstrated by axisymmetric bodies when compared with equivalent two-dimensional bodies.

Figure 3 presents typical results from wake pitot and static pressure surveys in a vertical plane through the model centerline. Flow development in the wake outside of the recirculation region is shown by means of Mach number profiles in the upper portion of the figure. The experimental data are compared with a prediction of wake thickness and zero-velocity line position from a theory developed by Mehta.[5] The theory is an integral method for solution of the fully turbulent, adiabatic near-wake field behind axisymmetric bluff-base bodies in supersonic flow. Figure 3 shows excellent agreement between this theory and the experimentally determined wake thickness. The zero velocity line also matches well with experiment upstream of the theoretically predicted rear stagnation point.

The radial surveys reveal a slight asymmetry in the base flow which may suggest a minor redefinition of the rear stagnation point location. It was found that, in the vertical plane, the true wake centerline is displaced upwards such that a zero velocity point persists in the Mach number profile back to approximately 8.9 cm from the base. This represents a 0.5-cm axial shift in rear stagnation point from that determined by model centerline measurements. The true wake centerline offset at 8.9 cm from the base is 0.19 cm.

Radial static pressure surveys in the base flow region are shown in the lower portion of Fig. 3. The variation from centerline pressure with increasing radius is consistent with streamline curvature as the flow initially converges toward

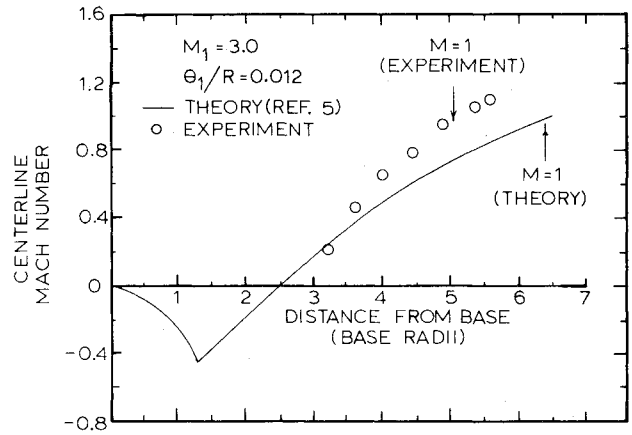

Fig. 5 Comparison of experimental near-wake centerline Mach number distribution with theoretical prediction—constant-area test section (zero external compression).

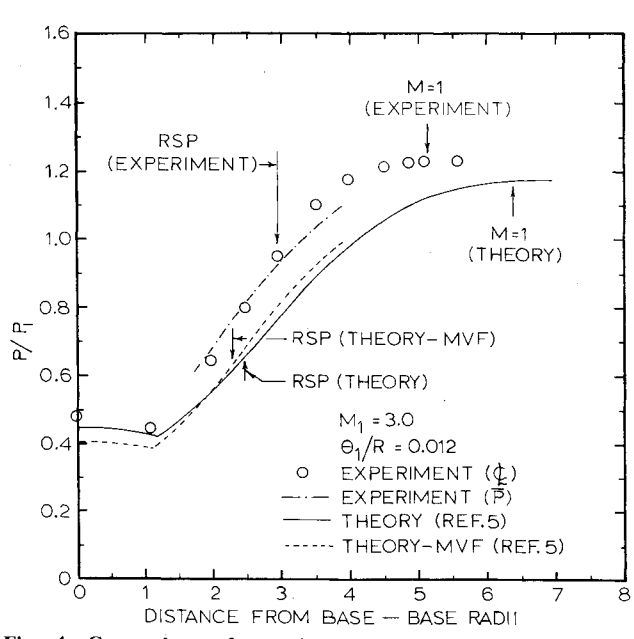

Fig. 4 Comparison of experimental near-wake centerline static pressure distribution with theoretical prediction—constant-area test section (zero external compression).

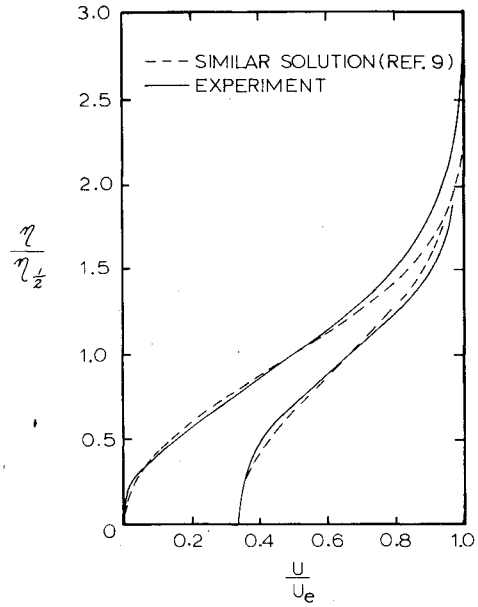

Fig. 6 Comparison of experimental and similar solution velocity profiles—constant-area test section (zero external compression).

Table 1 Tabulation of radius, Mach number, and static pressure distributions for external compression test section ducts

	Compression section								
	I			II			III		
X cm	R cm	M	$P/P_{01}\times10^2$	R cm	M	$P/P_{01}\times10^2$	R cm	M	$P/P_{01}\times10^2$
0	7.592	2.980	2.805	7.592	2.980	2.805	7.592	2.980	2.805
1.270	7.584	2.944	2.962	7.582	2.923	3.057	7.562	2.795	3.713
2.540	7.562	2.909	3.122	7.539	2.834	3.499	7.430	2.599	5.019
3.810	7.526	2.873	3.297	7.457	2.763	3.869	7.234	2.503	5.826
5.080	7.473	2.837	3.483	7.348	2.713	4.210	7.023	2.498	5.871
6.350	7.407	2.799	3.690	7.226	2.680	4.429	6.838	2.581	5.161
7.620	7.330	2.793	3.724	7.094	2.663	4.547	6.721	2.725	4.133
8.890	7.259	2.787	3.759	6.965	2.662	4.554	6.673	2.836	3.488
10.160	7.181	2.779	3.805	6.845	2.679	4.436	6.665	2.892	3.204
11.430	7.107	2.773	3.840	6.741	2.713	4.210	6.678	2.925	3.048
12.700	7.033	2.766	3.881	6.665	2.760	3.917	6.703	2.945	2.957
13.970	6.957	2.758	3.929	6.617	2.820	3.574			
15.240	6.883	2.749	3.984	6.604	2.883	3.248	6.772	2.965	2.869
16.510	6.810	2.749	3.984						
17.780	6.746	2.768	3.870	6.640	2.943	2.966	6.853	2.974	2.831
19.050	6.695	2.798	3.696						
20.320	6.668	2.829	3.525	6.715	2.965	2.869	6.942	2.977	2.818
21.590	6.657	2.867	3.328	6.761	2.969	2.852	6.988	2.977	2.818

and then turns back parallel with the axis. It should be noted that radial static pressure variations in the inner, lower velocity region of the shear flow are small when compared with the axial gradients.

Figures 4 and 5 compare the theory of Mehta with the present experimental centerline results for static pressures in the near wake and for flow acceleration aft of the rear stagnation point (RSP). The slightly higher experimental base pressure in Fig. 4 can be attributed to a small compression field initiated by the presence of a boundary layer on the outer duct. Both the experimental centerline static pressure data and a curve of the area-weighted mean static pressure $\bar{P}$ have been included on the figure to show the small but significant effect of radial pressure gradients in the shear layer. The centerline static pressure distribution is predicted using two forms of Mehta's theory. The basic theory employs a standard compressible eddy viscosity model in the shear regions. Mehta found, however, that a modified viscosity form (MVF) of the theory using an empirical initial freestream Mach number correction to the local eddy viscosity model yielded better correlation of experimental and theoretical results over a wider range of Mach numbers. In general, the analytical and experimental wake development shown in Figs. 4 and 5 agree well.

Figure 6 compares similar solutions for incompressible axisymmetric wakes[9] with two experimental velocity profiles. The experimental data radial coordinates are transformed to the incompressible form using a Stewartson-type transformation. These similar profiles and a set of nearly indistinguishable cosine profiles were both employed in Mehta's integral theory using a Stewartson-type transformation to account for compressibility. The experimental velocity profiles are in reasonably good agreement with the analytical representations. It is apparent that excellent agreement over the major portion of the profile would be obtained if the centerline of the experimental data were shifted slightly so as to match experimental and analytical velocity gradients at the half-velocity point.

External Disturbance Studies

After completion of the base flow studies in an undisturbed freestream, the test section was modified for investigating the characteristics of the near wake under the influence of externally imposed compression. These tests were designed to determine the control of and changes in the near-wake scales and flow features afforded by external compression and to provide data under well defined boundary conditions for testing near-wake theory. The external disturbances were chosen to provide a reasonable simulation of those due to burning in the freestream but without the complications of combustion-zone alterations due to waves from the near wake. Replacement of the original constant-area test section with a series of converging ducts provided these freestream compression fields focused on the near wake. Thus, the simulated burning zone is about 1.7 base radii outside the wake rather than close to the wake as in the case of practical external burning.

The initial contour (Compression Sec. I) was designed to impose a pressure field on the wake that would approximately eliminate base drag. This contour simulates a free-flight streamline along the lower boundary of a simple, one-dimensional, heat-addition zone 8.44 base radii in length and, initially, 0.27 base radii in annular thickness. Curvature due to the heat-addition zone being immersed in an axisymmetric supersonic flow is accounted for. The heat release is modeled by a cosine curve simulating the slow rise and tailoff of combustion.

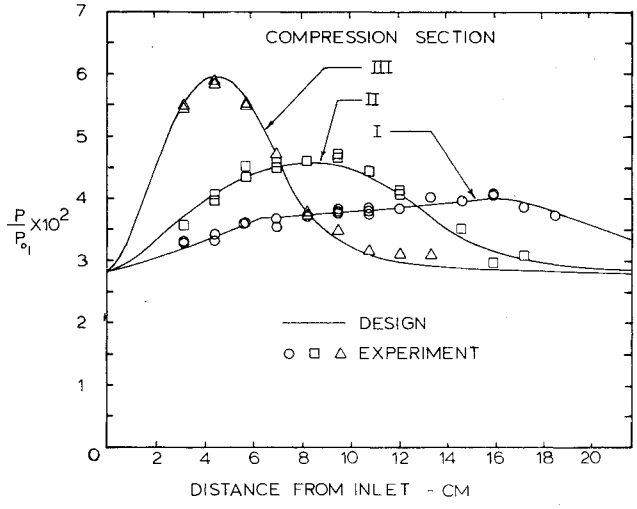

Fig. 7 Comparison of external compression test section design and performance.

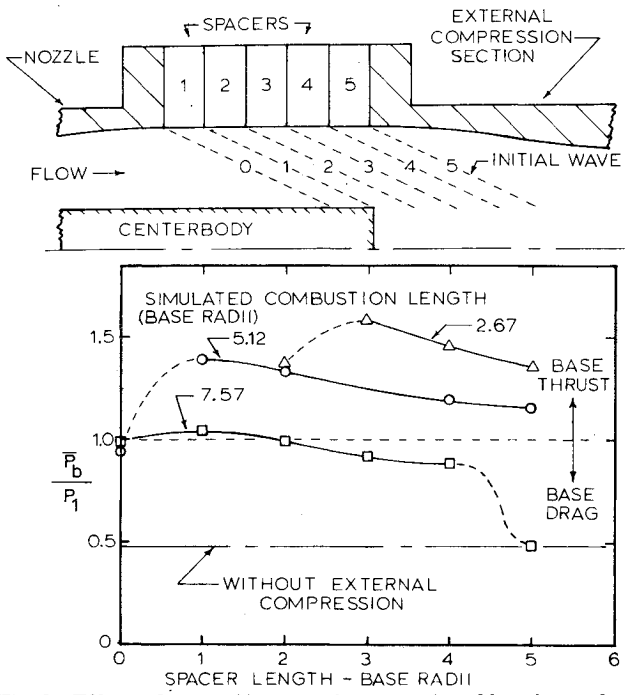

Fig. 8 Effects of external compression strength and location on base pressure.

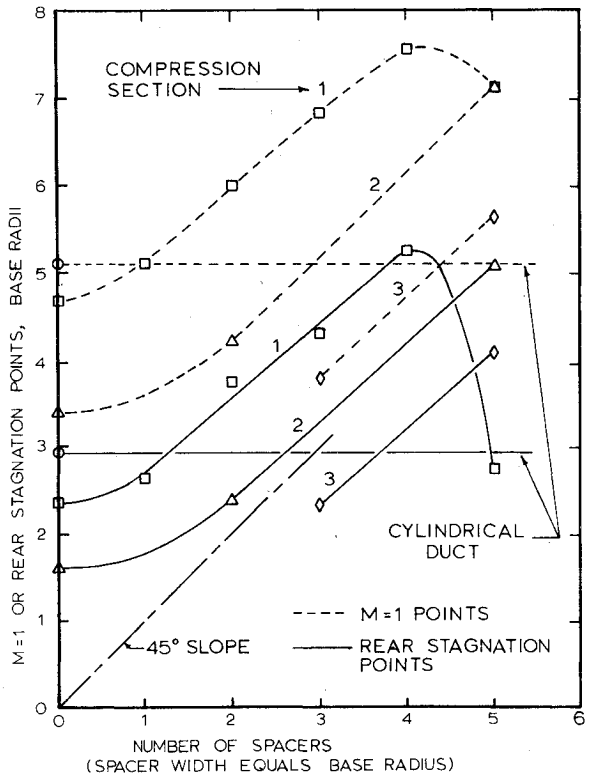

Fig. 9 Effects of external compression strength and location on near-wake scales.

Two subsequent alternate test section contours were then designed to simulate an identical total heat addition at increased release rates. A fourth test section was constructed using six symmetrically located half-bodies of revolution attached to the inner wall of a cylindrical duct. The axial area distribution of this section was identical to that of the second axisymmetric compression section and was included to study the effects of equivalent heat addition in discrete plumes.

A series of five spacer rings were constructed to allow axial translation of the external disturbance ducts relative to the

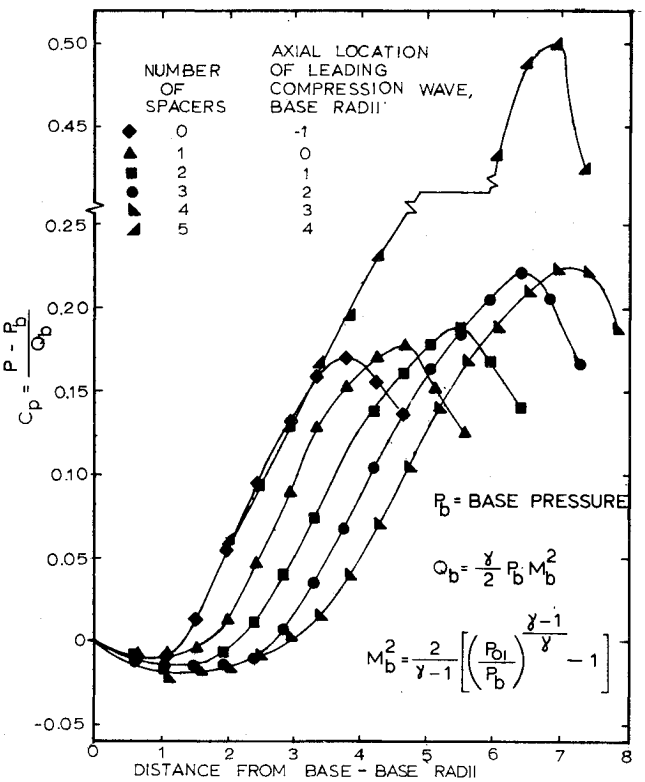

Fig. 10 Effects of external compression location on centerline pressure distribution—Compression Sec. I.

model. The inside diameter of the rings match the exit diameter of the nozzle and are inserted between the nozzle exhaust and the compression section inlet. Use of the spacers provides for translation of the external disturbance in increments of one base radius.

Finally, an alternate base plate was fabricated for modeling the solid body blockage of discrete radial fuel jets exhausting near the base. The jets were simulated with six solid cylindrical pegs fixed on the model perimeter to allow study of blockage effects without the complication of actual mass injection.

Axisymmetric Disturbance Test Results

The design and performance of each axisymmetric compression duct are shown, respectively, in Table 1 and Fig. 7. Table 1 tabulates the axial distribution of design radius, Mach number, and static pressure. Boundary-layer growth has been accounted for in the Mach number and static pressure values. The design pressures are plotted in Fig. 7 and are shown to be in good agreement with typical static pressure measurements on the duct surface.

The test configuration for external compression is shown in Fig. 8 along with resulting base pressure measurements. The initial, mild contour (Compression Section I) performed as designed by approximately eliminating base drag. A weak optimum axial location is shown for this case when the compression has been displaced downstream by one base radius. Base pressure falls slightly with the insertion of additional spacers up to a total of four. Base pressure, however, returns sharply to the value measured with a constant area duct when the fifth spacer is introduced. For this case, the initial compression wave intersects the wake downstream of the sonic point and can no longer influence the base region.

Translation of the two alternate axisymmetric disturbance sections verified the base flow trends shown with the original compression duct. As the compression severity increases, the optimum location of each duct moves downstream and the corresponding maximum base pressure rises. The rearward shift in optimum location probably results from the

steepening of compression waves due to coalescence. Finally, Fig. 8 shows that the third, most severe compression rate duct yields an elevation in the base pressure sufficient to completely neutralize drag on a well designed projectile for which base and wave drag are typically comparable.

The systematic variation of disturbance position and strength revealed two additional characteristic lengths inherent in base flows with external compression. As shown in Fig. 9, the wake length scales vary directly with location of the compression surfaces. Thus, movement of the disturbance field downstream tends to lengthen the distances from the base to the rear stagnation and sonic velocity points. Conversely, as the compression strength increases by decreasing the compression length for a fixed location, the wake length decreases.

Figure 10 further illustrates the direct relation of wake length to disturbance location for the initial, relatively mild compression surface. For those cases in which the compression field tends to elevate base pressure, the normalized centerline static pressure distributions clearly reflect disturbance location. The trend terminates abruptly, however, for the five-spacer case when base pressure reverts to the no-compression value.

Radial and axial measurements of Mach number and static pressure in the wake for the initial compression section with no spacers are shown in Fig. 11. Comparison of the Mach number profiles for this case with those presented in Fig. 3 for the cylindrical duct illustrates a slightly fuller and shortened recirculation region reflecting the elevated base pressure. As in Fig. 3, the static pressure profiles in Fig. 11 indicate the effects of flow curvature. In general, the radial pressure variation magnitudes are larger for the compression case resulting from the increased severity of turning associated with the shorter wake.

Discrete Disturbance Test Results

In actual practice, external burning to influence base pressure would most likely take place in discrete plumes originating from radial fuel injection nozzles located near the projectile base. As mentioned previously, a fourth test section employing six half-bodies of revolution was fabricated to compare the effects of discrete and equivalent axisymmetric disturbances. The axial area distribution of this fourth section was identical to that of the second compression duct (II).

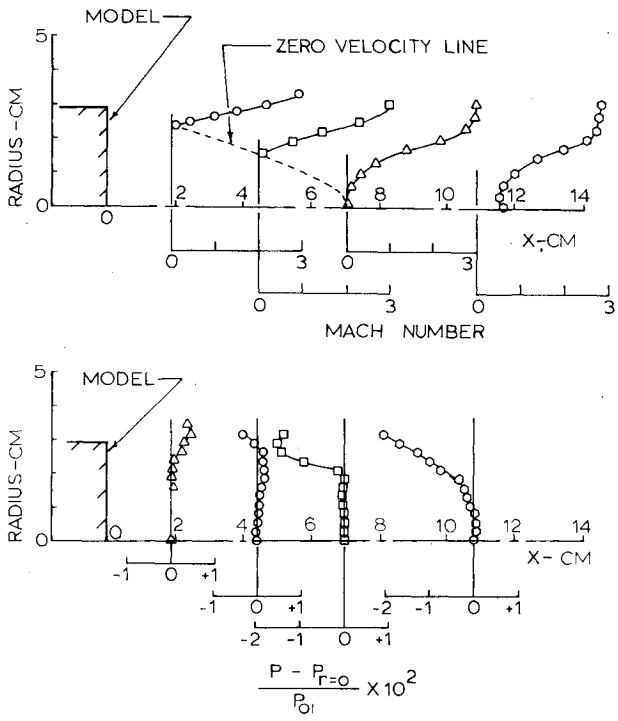

Fig. 11 Near-wake radial Mach number and static pressure distributions—Compression Sec. I, zero spacers.

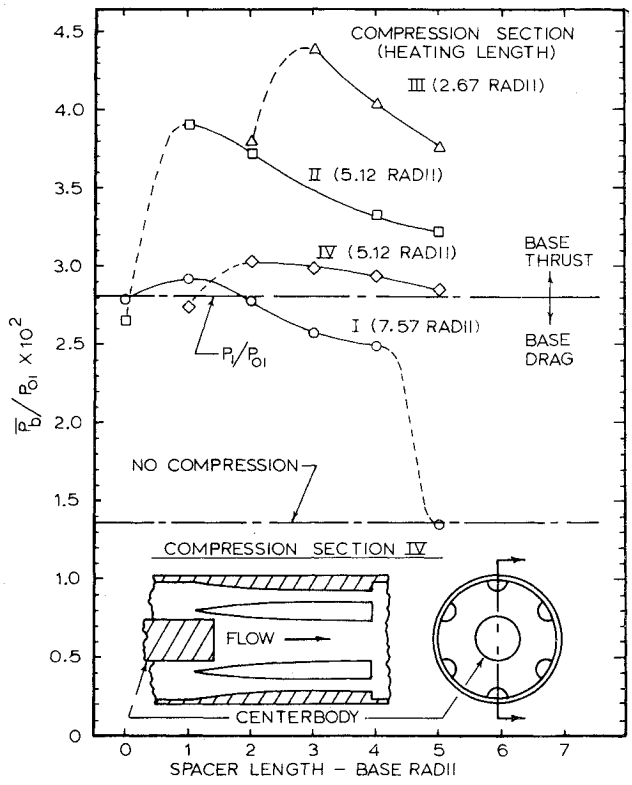

Fig. 12 Comparison of base pressure for axisymmetric and equivalent discrete compression (Secs. II and IV).

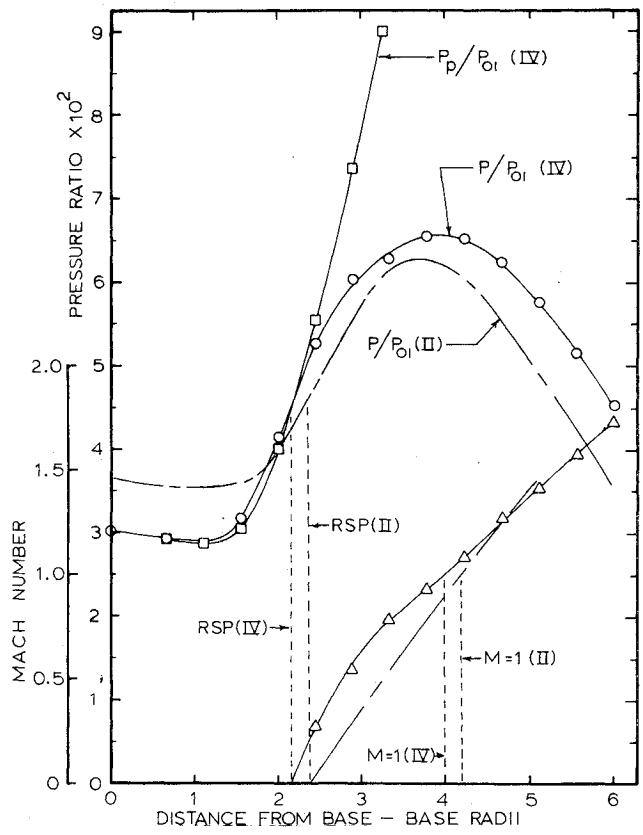

Fig. 13 Comparsion of near-wake centerline pressure and Mach number distributions for axisymmetric and equivalent discrete compression (Secs. II and IV).

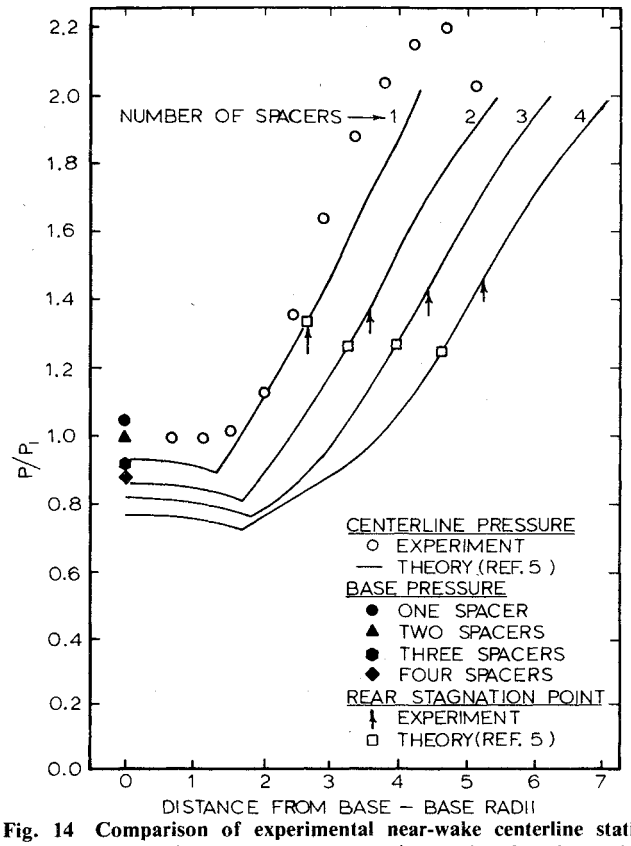

Fig. 14 Comparison of experimental near-wake centerline static pressure distribution and rear stagnation point location with theoretical prediction—Compression Sec. I.

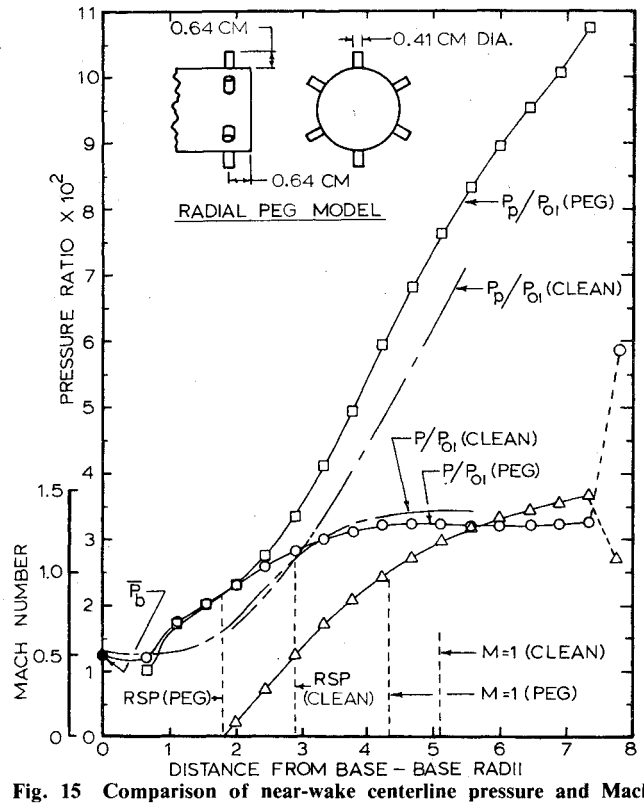

Fig. 15 Comparison of near-wake centerline pressure and Mach number distributions for clean base and peg base (simulated discrete radial jet blockage).

Figure 12 schematically shows the fourth compression section along with base pressure test results for various axial duct locations. A significant reduction in base pressure from the axisymmetric case is seen at any given duct position. Figure 13 compares centerline static pressure and Mach number distributions for the axisymmetric and discrete disturbance ducts with two spacers. It is clear that, in addition to reducing base pressures, use of discrete disturbances has moved the rear stagnation point forward and has mildly increased the peak centerline static pressure.

It is believed that an explanation for the somewhat deteriorated performance just described may be found in a secondary vorticity field created by the discrete disturbance contours. Static pressure measurements along the duct and centerbody surfaces between half-bodies revealed considerably higher values than for the axisymmetric compression section (II). These higher wall pressures are due to coalescence of waves from adjacent contours and indicate the existence of strong peripheral pressure gradients in the freestream. Zones of higher pressure existing between half-bodies alternate with regions of lower pressure directly over the bodies and create the potential for streamwise secondary vorticity in the wake shear flow. The resulting increased mixing most certainly influences wake development by thickening and energizing the shear layer so as to increase its ability to oppose recompression. Since the maximum static pressure for the axisymmetric and discrete compression cases is nearly the same, base pressure for the discrete disturbance case must adjust downward to accommodate the increased pressure rise. It should be noted, however, that even though base pressure is lower for the discrete disturbance case, the base drag has still been neutralized.

Figure 14 compares Mehta's theory with measurements in the wake for the first compression section. Agreement in centerline static pressure distribution and location of the rear stagnation point for one spacer is quite good. Some deterioration in matching is reflected by disagreement in the measured and predicted rear stagnation point location as the wake is stretched by the addition of spacers. Predicted base pressure for all four cases shown is 10-15% below the experimental values.

Figure 15 presents the centerline pressure and Mach number distribution from the peg base tests. Results from the "clean" base tests are also provided to show changes in the wake structure. It is apparent that the presence of the pegs has significantly shortened the wake. Also, the base pressure determined from a simple average of seven taps, is about 8% lower than the clean base configuration value of $\bar{P}_B/P_{0l} = 1.36 \times 10^{-2}$. The sharp rise in centerline static pressure and the corresponding drop in Mach number as indicated by the last data point on Fig. 15 is attributed to reflections from the outer wall of the separation shocks created by the pegs. This location agrees with that estimated by tracing compression waves from static pressures measured on the centerbody ahead of the pegs and on the outer cylinder. Since this interaction occurs downstream of the point where the wake is supersonic, any effect of tunnel interference is ruled out. The reduction in the base pressure and the change in the base flow structure is thought to be primarily a result of increased mixing due to streamwise secondary vorticity generated by the pegs.

Summary

The present experiments simulating external burning have shown that substantial base thrust can be obtained by imposing axisymmetric or asymmetric compression on the turbulent near-wake region of a projectile in supersonic flight. Systematic variations in disturbance strength and axial position revealed that the length scales of these compressions are reflected in the wake structure. As expected, base pressure rises and the near wake shortens with increasing compression severity for any particular axial disturbance location. Downstream translation of a given disturbance acts to lengthen the wake and yields a mild optimum base pressure for that disturbance. The present tests demonstrate a case in

which base pressure elevation is sufficient to completely neutralize base and forebody drag on a well designed projectile.

In actual practice, external burning will probably take place in discrete plumes originating from radial injection of fuel in the vicinity of the base plane. Tests simulating this configuration showed that base pressure elevation is significantly reduced for discrete externally generated disturbances when compared with the equivalent axisymmetric compression. The loss in base thrust is apparently related to streamwise vorticity created in and above the shear layer by the nonuniform external compression field. The present tests demonstrated, however, that base pressure had still been boosted sufficiently to eliminate base drag.

Finally, modeling of the solid body blockage effects of discrete radial fuel jets near the base showed relatively large changes in the near-wake length scales. Despite the alteration in wake structure, base pressure was only slightly lower than for a "clean" projectile with no radial jet modeling.

References

[1] Strahle, W.C., "Theoretical Consideration of Combustion Effects on Base Pressure in Supersonic Flight," *Twelfth Symposium on Combustion,* Combustion Institute, Pittsburgh, Penn., 1969, pp. 1163-1173.

[2] Smithey, W.J.H., "Projectile Thrust-Drag Optimization with External Burning," Ph.D. Thesis, Naval Postgraduate School, Monterey, Calif., June, 1974.

[3] Crocco, L. and Lees, L., "A Mixing Theory for the Interaction Between Dissipative Flows and Nearly Isentropic Streams," *Journal of Aerospace Sciences,* Vol. 19, Oct. 1952, pp. 649-676.

[4] Peters, C.E. and Phares, W.J., "Analytical Model of Supersonic Turbulent Near-Wake Flows," Arnold Engineering Development Center, Arnold Air Force Station, Tenn., AEDC-TR-76-127, Sept. 1976.

[5] Mehta, G.K., "A Theory of the Supersonic Turbulent Axisymmetric Near Wake Behind Bluff-Base Bodies," Ph.D. Thesis, Georgia Institute of Technology, Atlanta, Ga., June 1977.

[6] Ward, J.R., Baltakis, F.P., Elmendorf, T.A., and Mancinelli, D.J., "Wind Tunnel Experiments of the Effect of Near-Wake Combustion on the Base Drag of Supersonic Projectiles," U.S. Army Ballistic Research Laboratory, Memorandum Rept. No. 2588, Feb. 1976.

[7] Murthy, S.N.B. and Osborn, J.R., "Base Flow Control with Combustion at Supersonic Velocities," U.S. Army Ballistic Research Laboratory, Contract Rept. No. 309, Aug. 1976.

[8] Schadow, K.C. and Chieze, D.J., "Effect of Injector Design on External Burning of Solid Propellants in Mach 2 Airstream," Naval Weapons Center, Tech. Publ. 5917, Feb. 1977.

[9] Kubota, T., Reeves, B.L., and Buss, H., "A Family of Similar Solutions for Axisymmetric Incompressible Wakes," *AIAA Journal,* Vol. 2, Aug. 1964, pp. 1493-1495.